Surface normal rotation: a new technique for grazing-incidence monochromators

Michael C. Hettrick

Applied Optics Vol. 31, Issue 34, pp. 7174-7178 (1992)

http://dx.doi.org/10.1364/AO.31.007174

Surface normal rotation: a new technique for grazing-incidence monochromators

Michael C. Hettrick

Hettrick Scientific Inc., P.O. Box 8046, Kensington, California 94707.
Received 13 July 1992.
0003-6935/92/347174-05$05.00/0.

A class of fixed-slit monochromator that scans wavelength over a broad region using a grazing-incidence diffraction grating that rotates about its surface normal is described.

Key words: *Monochromators, diffraction gratings, grazing incidence, x-ray optics.*

Grating rotation was previously used for selecting wavelength only when the rotation axis lay within the surface of the grating.[1–8] In classical diffraction this axis is also parallel to the grooves, and the rotation alters the image distance of any focusing grating because of the change in the angles of incidence and diffraction. This effect is most pronounced at the grazing angles of incidence that are necessary for broadband reflectance in the soft x ray. Even with the use of varied groove spacings[9–11] to overcome this effect, gratings rotated about their grooves cause a wavelength-dependent change in the numerical aperture, which results in a nonideal illumination of targets to which the diffraction radiation is directed. In the past a constant numerical aperture required an effective slit movement along the Rowland circle[12] or approximations thereto.[13]

As an alternative, consider a rotation of a diffraction grating about an axis normal to its surface, as depicted in Fig. 1(a). The grooves are illustrated to be initially normal to the incident principal ray. If the grating is now rotated by an angle θ, the incident rays view a groove spacing that has increased by $1/\cos\theta$. When fixed slits are used, the scanned wavelength is to a good approximation given by

$$\lambda = \lambda_0/\cos\theta \tag{1}$$

with fixed angles of incidence α and diffraction β, where

$$\lambda_0 = (\sin\beta - \sin\alpha)d_0/m \tag{2}$$

is the minimum accessible wavelength in spectral order m.

Remarkably this simple scan motion has not hitherto been proposed. At near normal incidence such a grating rotation would admittedly result in a large deflection of the diffracted radiation along the length of the slit and a blurred image on a fixed image plane. However, in the limits of grazing incidence, these effects are found to vanish unexpectedly. In this case the optical aberration can be derived simply by reference to Fig. 1(b). If the incident radiation diverges (or converges) by an angle ϕ in the (sagittal) y direction, the extremum rays will view slightly different spacings at a nonzero value of 0. For grooves that are straight and parallel, this results in a wavelength aberration,

$$\Delta\lambda/\lambda = \phi\tan\theta, \tag{3}$$

diffracted through an infinitesimal width slit that is oriented parallel to the grating surface. For example, consider $\phi = 1$ mrad. Over an octave in wavelength, Eq. (1) specifies a maximum rotation angle of $\theta = 60°$, for which Eq. (3) results in an aberration of only $\sim 1/600$.

A second effect of the proposed grating rotation is that the image will be deflected by an amount y along the length of the slit:

$$y/r' = (m\lambda_0/d_0)\tan\theta, \tag{4}$$

where r' is the focal length of the grating. For a groove spacing of 1/500 mm and a minimum wavelength of 1 nm, this deflection is $y/r' = 0.88$ mrad at a rotation angle of 60°. As Eq. (4) indicates, the magnitude of this deflection scales with the ratio of wavelength-to-groove spacing, which becomes exceedingly small in the limit of grazing incidence.

Another property of the rotation is that the effective groove spacing, namely, that viewed by the incident radiation, increases in exact linear proportion to the selected wavelength as given by Eq. (1). First, this results in a constant resolving power $(\lambda/\Delta\lambda)$ for set slit widths. Second, there is no maximum (horizon) wavelength that is analogous to the classical rotation limit. The increased groove spacing maintains the blazed wavelength λ_B near the selected wavelength λ. Geometrically one finds that in surface normal rotation,

$$\lambda_B/\lambda = [1 - (1 - \lambda_0/\lambda)\delta_0/\gamma_0]\lambda_0/\lambda; \tag{5}$$

in classical rotation,

$$\lambda_B/\lambda = \lambda_0/\lambda - (1 - \lambda_0/\lambda)\delta_0/\gamma_0, \tag{6}$$

where δ_0 is the blaze angle of the assumed triangular grooves, and γ_0 is the grazing angle relative to the groove facets at λ_0 where $\lambda_B = \lambda$. Figure 2 compares the two cases for $\delta_0/\gamma_0 = 1/3$. In addition the new scheme rotates the groove facets out of the highly shadowed condition endemic to the classical method, resulting in further increases in relative efficiency. According to theory[14] the relative diffraction efficiency ϵ_B at the blazed wavelengths given above equals the fraction of the groove that is unshadowed. For the two cases in surface normal rotation,

$$\epsilon_B = (\gamma_0/\delta_0 - 1)/(\gamma_0/\delta_0 - 1 + 2\lambda_0/\lambda); \tag{7}$$

in classical rotation,

$$\epsilon_B = (\gamma_0/\delta_0 - \lambda/\lambda_0)/(\gamma_0/\delta_0 - \lambda/\lambda_0 + 2). \tag{8}$$

For example, as plotted in Fig. 2, for $\delta_0/\gamma_0 = 1/3$ classical rotation results in complete shadowing at a horizon wavelength equal to three times the blazed wavelength. In contrast, rotation about the surface normal decreases the shadowing to zero as the rotation approaches $\theta = 90°$. While it is not maintained on blaze through the scan, it is

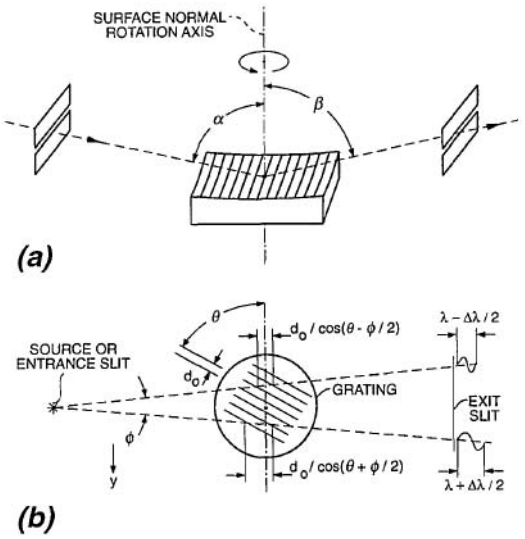

Fig. 1. Geometry of a simple surface normal rotation (SNR) fixed-slit grating monochromator. (a) Three-dimensional perspective where the grating is oriented to diffract the minimum wavelength through the exit slit. (b) Top view of the rotated grooves showing the groove spacings projected upon the sagittal incident rays, resulting in a limit to the spectral resolution. The same rotation scan technique may be used to construct other optical systems including plane grating designs, those employing auxiliary mirrors, and those where the slit(s) may move.

clear that the new scheme will exhibit a broad diffraction efficiency curve.

To test the above theories, a soft-x-ray vacuum monochromator has been constructed. It consists of a slitless laser-produced plasma source, a selectable series of knife-edge sagittal apertures, a palladium-coated concave grating with a 20-m radius of curvature and a ruled area of 32 mm × 32 mm, and a selectable series of exit slits. The instrument length from source to exit slit is $r + r'$, ~1.5 m, the angular separation between the diffracted and incident rays is ~4°, and the minimum wavelength is ~1.04 nm. While the new scan technique is not specific to any particular focusing condition, the source and exit slits were located approximately on the grating Rowland circle. A silicon photodiode detector (10 mm × 10 mm) was placed at the output end of the exit slit to monitor the transmitted current as a function of the grating scan angle driven by a microstepped motor residing outside of the vacuum. The rotation angle values were then converted to absolute wavelength by use of Eq. (1) and one known line in the spectrum.

Figure 3 presents spectra of various laser targets (aluminum, brass, and stainless steel) taken by the new SNR monochromator. It shows numerous lines and continua extending from the minimum wavelength (~1 nm) to ~20 times this value. However, as predicted, the spectral aberration increases at long wavelengths because of the large rotation angle combined with a sagittal aperture of 2 mrad.

According to theory high resolution can be obtained by reducing the sagittal aperture. In Fig. 4 a spectrum of the stainless-steel target was obtained with a sagittal baffle of 1 mrad. Equation (3) determines the fractional optical aberration to be 1/730 at 1.7 nm, 1/250 at 4.1 nm, 1/140 at 7.1

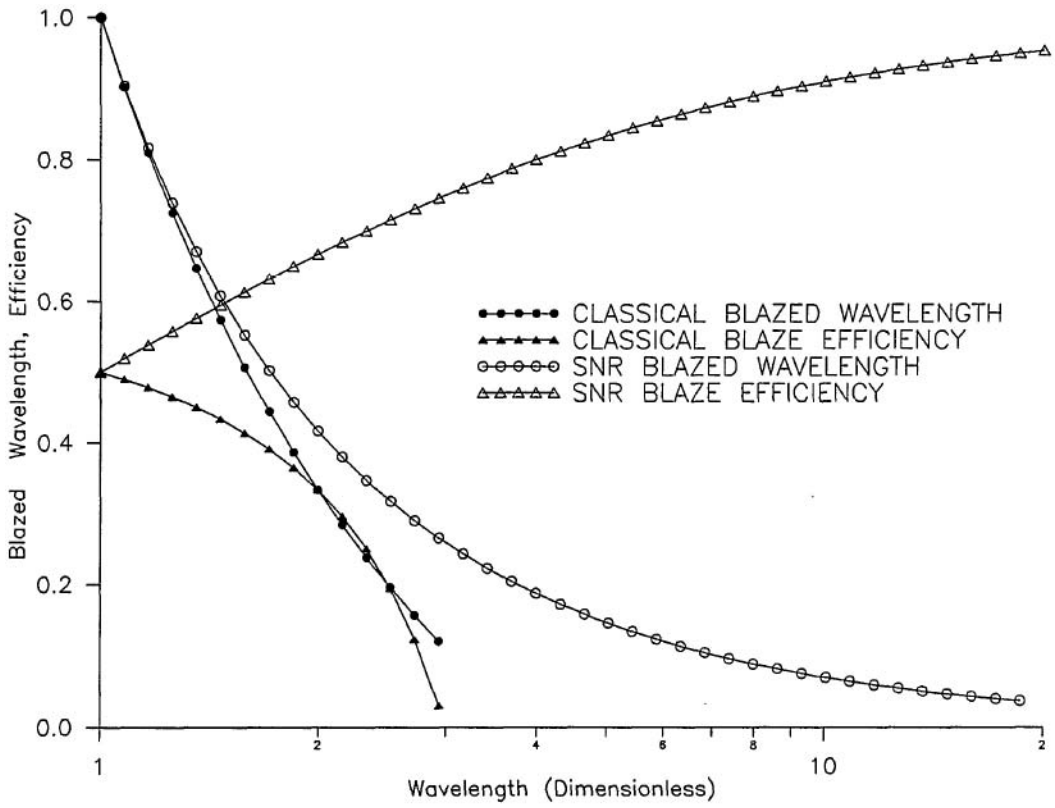

Fig. 2. Geometrical calculations of the blazed wavelength and relative diffraction efficiency at that wavelength. The horizontal axis is the selected wavelength (divided by the minimum wavelength) emerging from the exit slit. The blazed wavelength values are normalized to the value of the selected wavelength.

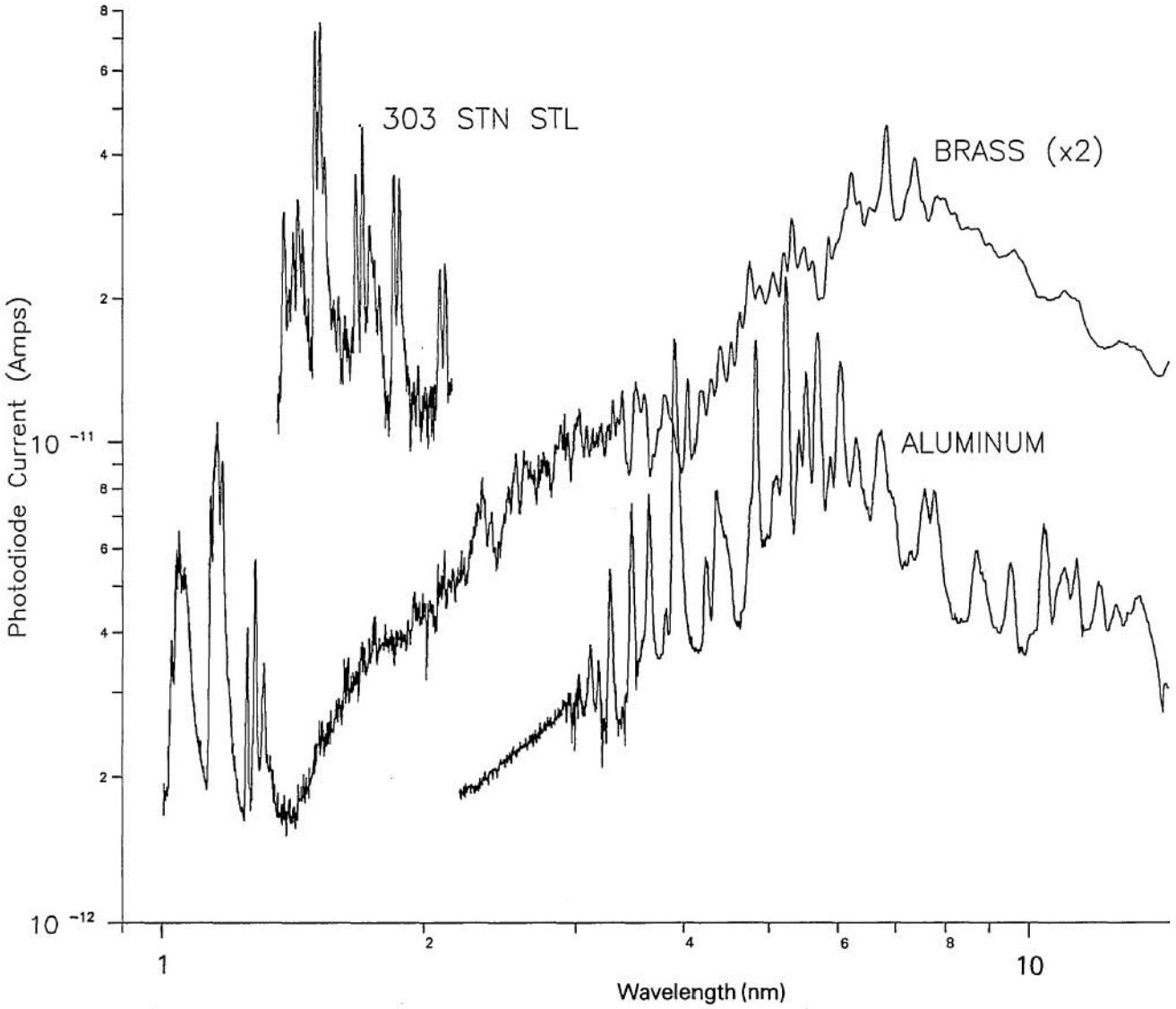

Fig. 3. Survey spectra of various laser-produced plasmas obtained when a 2-mrad sagittal aperture and a 50-μm exit slit are used. The slit width limits the resolution at short wavelengths, and the image tilt limits the resolution at the long wavelengths. The falloff in throughput at the long wavelengths is believed to be at least partly a result of the diffracted rays' being deflected off the edge of the silicon photodiode detector.

nm, and 1/66 at 15.8 nm. When the blur of ~1/360 caused by the exit slit width (20 μm) and comparable source size is added, the resulting predicted net aberrations of 1/290 at 1.7 nm, 185 at 4.1 nm, 117 at 7.1 nm, and 1/60 at 15.8 nm are in good agreement with the measured linewidth values of 1/335 at 1.7 nm, 1/149 at 4.1 nm, 1/118 at 7.1 nm, and 1/66 at 15.8 nm. The effect of sagittal aberration can be entirely eliminated, and the resolution is limited only by slit widths, if a mirror preceding the grating is used to collimate incident radiation in the sagittal direction [$\phi = 0$ in Eq. (3)].

Another method of removing the optical aberration is to tilt the exit slit as a function of wavelength. From Fig. 1(b) it is clear that the aberrant dispersion varies linearly along the length of the grooves, resulting in an image that, although tilted relative to the grating surface, remains narrow. From Eq. (3) the required slit tilt is

$$\psi = (m\lambda_0/d_0)\tan\theta/(1 + r_y/r')/\cos\beta. \qquad (9)$$

For example, in the prototype monochromator the image tilt is ~6° at 15.8 nm, where the rotation angle θ is ~86°. When the sagittal aperture ϕ is set to 4 mrad, a slit that is parallel to the grating surface results in an optical aberration of 0.95 nm as confirmed by the measured result inset of Fig. 4. Manually tilting the exit slit by 6° to match the image tilt canceled this aberration, and a spectral resolution of 0.15 nm limited by the exit slit width of 50 μm is measured. It is also clear that the grating could be tilted with the slit(s) fixed in orientation to achieve similar correction. A SNR monochromator whose slit(s) or grating additionally rotates in this sense can be forced in continuous focus as the grating is simultaneously rotated about its surface normal to scan the wavelength. Yet another method that can be used to reduce the image tilt, without resorting to rotating slits, is to curve the grating grooves toward the source of diverging radiation. This decreases the variation in effective spacings seen along the length of the straight grooves illustrated in Fig. 1(b).

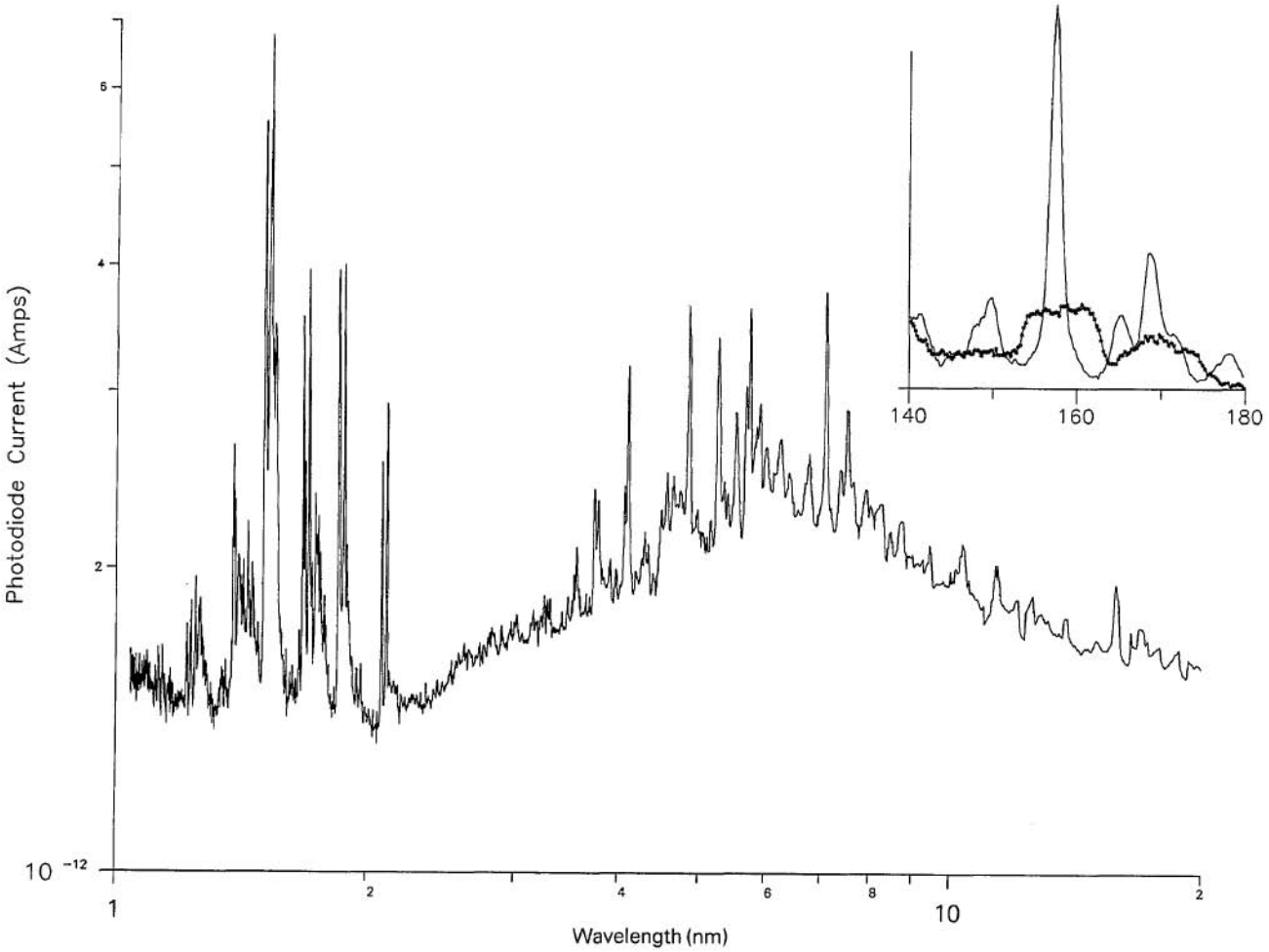

Fig. 4. Higher-resolution spectrum of a type 303 stainless-steel target obtained by using a sagittal aperture of 1 mrad and an exit-slit width of 20 μm. The heavy curve in the inset shows the degradation caused by an increased (4-mrad) sagittal aperture. The light curve in the inset shows a factor-of-6 improvement obtained by tilting the exit slit for optimum performance at a wavelength of 15.8 nm.

Calculations reveal a factor-of-4 decrease in the maximum amount of image tilt that is possible over a factor of 4 in scanned wavelength.

While in the prototype SNR monochromator the grating rotation is driven by a worm gear, a linear wavelength mechanism is also simple to construct. Consider a ball-ended bar that is parallel to a plane pusher plate when the grating rotation angle $\theta = 90°$. Then the linear travel x of the pusher divided by the pivot length L of the bar is equal to $\cos\theta$. Thus, to within the accuracy of Eq. (1), this cosine bar is complementary to the well-known sine bar of classically rotated gratings, but now results in linearity with the frequency of the photon emerging from the exit slit:

$$\nu/\nu_0 = x/L \qquad \text{or} \qquad \lambda/\lambda_0 = L/x. \tag{10}$$

Another useful property of rotation about the grating surface normal is that the zero-order image is fixed in position throughout the scan. A slit placed at this location can be used to transmit the longer-wavelength radiation not efficiently diffracted by the grating. The emerging energy can be fed into a monitor or even to a series network of monochromators.

Because of the simple rotation scheme and mechanisms, the SNR monochromator is ideal for use in high and ultrahigh vacuum. Hettrick Scientific, Inc., holds the license for the manufacture, sale, and use of such devices. A patent is pending on spectroscopic instruments based on the general technique of surface normal grating rotation, one example of which was described in this Technical Note.

References

1. M. Seya, "A new mounting of concave grating suitable for a spectrometer," Sci. Light **2,** 8–17 (1952).
2. R. Onaka, "Grating mounting for vacuum ultraviolet monochromator," Sci. Light **7,** 23–27 (1958).
3. R. P. Madden and D. L. Ederer, "Stigmatic grazing-incidence monochromator for synchrotrons," J. Opt. Soc. Am. **62,** 722 (A) (1972).
4. H. Dietrich, "A grazing incidence vacuum ultraviolet monochromator with fixed exit slit," Rev. Sci. Instrum. **43,** 434–442 (1972).
5. H. Petersen, "The plane grating and elliptical mirror: a new optical configuration for monochromators," Opt. Commun. **40,** 402–406 (1982).
6. W. R. Hunter, R. T. Williams, J. C. Rife, J. P. Kirkland, and M. N. Kabler, "A grating/crystal monochromator for the spectral range 5 eV to 5 keV," Nucl. Instrum. Methods **195,** 141–153 (1982).
7. W. C. Cash, Jr., "X-ray spectrographs using radial groove gratings," Appl. Opt. **22,** 3971–3976 (1983).

8. M. C. Hettrick and J. H. Underwood, "Stigmatic high throughput monochromator for soft x rays," Appl. Opt. **25,** 4228–4237 (1986).
9. M. C. Hettrick, "High resolution gratings for the soft x ray," Nucl. Instrum. Methods **A266,** 404–413 (1988).
10. M. Itou, T. Harada, and T. Kita, "Soft x-ray monochromator with a varied-space plane grating for synchrotron radiation: design and evaluation," Appl. Opt. **28,** 146–153 (1989).
11. M. C. Hettrick, "In-focus monochromator: theory and experiment of a new grazing incidence mounting," Appl. Opt. **29,** 4531–4535 (1990).
12. F. C. Brown, R. Z. Bachrach, and N. Lien, "The SSRL ultrahigh vacuum grazing incidence monochromator: design considerations and operating experience," Nucl. Instrum. Methods **152,** 73–79 (1978).
13. E. Ishiguro, M. Suzui, J. Yamazaki, E. Nakamura, K. Sakai, O. Matsudo, N. Mizutani, K. Fukui, and M. Watanabe, "Constant deviation monochromator for the range 100 Å < λ < 1000 Å," Rev. Sci. Instrum. **60,** 2105–2108 (1989).
14. M. Neviere, D. Maystre, and W. R. Hunter, "On the use of classical and conical diffraction mountings for XUV gratings," J. Opt. Soc. Am. **68,** 1106–1113 (1978).

Thermal apparent-strain sensitivity of surface-adhered, fiber-optic strain gauges

Tomas Valis, Dayle Hogg, and Raymond M. Measures

Institute for Aerospace Studies, University of Toronto, Downsview, Ontario M3H 5T6, Canada.
Received 16 December 1991.
0003-6935/92/347178-02$05.00/0.

We have derived, based on established practice in experimental mechanics, an equation for calculating the thermal apparent-strain sensitivity of phase-modulated, surface-adhered, fiber-optic strain sensors. This formulation permits the thermal performance of fiber-optic strain gauges to be compared with conventional resistive gauges. This sensitivity for commonly used fiber-optic sensors is summarized.
Key words: *Fiber-optic sensors, strain measurement.*

The cosensitivity to strain and temperature of phase-modulated fiber-optic sensors has been known and measured for more than a decade. More recently these sensors have been adhered to and embedded in structures for use as strain gauges. It is advantageous to apply widely used resistive-foil strain gauge concepts to the design of fiber-optic strain gauges. When using resistive-foil gauges, one is interested not in the unadhered temperature sensitivity but rather in the thermal apparent-strain sensitivity. This quantity is dependent on the properties of both the optical fiber and the host material. The formula for calculating the apparent strain of conventional strain gauges has been used for several decades. The following development yields the first-order thermal apparent-strain sensitivity for surface-adhered, phase-modulated, fiber-optic strain gauges. The purpose of this development is to permit fiber-optic strain gauges to be compared with their resistive-foil counterparts in a manner that is familiar to the experimental mechanics community.

An electrical strain gauge is said to generate a thermally induced apparent strain reading (apparent strain for short) if its resistance changes when it is adhered to an unconstrained structure subject to a temperature change. Converting the change in resistance to a change in strain (using the electrical strain gauge factor), one may quote an apparent-strain sensitivity in standard engineering units of με/K (1 με is 10^{-6} longitudinal deformations per unit length). The ideal is a zero apparent-strain sensitivity gauge. It generates a constant strain output if it is adhered to a heated, unconstrained structure. If adhered to a fully constrained, thermally loaded structure, the gauge generates an output that is proportional to the thermal stress. This type of response is associated with a self-temperature-compensated (STC) strain gauge.

In mathematical terms one begins by modifying Hooke's law to account for the stress-free thermally induced strain e_i. This generalized form is expressed as

$$\epsilon_i = \mathbf{S}_{ij}\sigma_j + e_i, \tag{1}$$

where $\mathbf{S}_{ij}$ is the compliance tensor.

It is useful to refer to a stress-related strain, which can be defined as $\epsilon_i^S \equiv \mathbf{S}_{ij}\sigma_j$.

The apparent strain ϵ_{appar} is defined as

$$\epsilon_{appar} \equiv \epsilon_{meas} - (\epsilon_i^S). \tag{2}$$

A STC sensor yields an output that is proportional to ϵ_i^S of the host structure.

Within the context of a first-order model, the following assumptions are made:

(1) The coupling tensor $\epsilon_i^f = \mathbf{Z}_{ij}\epsilon_j^h$ takes the form

$$\mathbf{Z}_{ij} = \begin{pmatrix} 1 & 0 & 0 \\ -\nu^f & 0 & 0 \\ -\nu^f & 0 & 0 \end{pmatrix}, \tag{3}$$

where ν is Poisson's ratio, 1 is the fiber direction, 2 and 3 are transverse directions, and superscripts f and h refer to the optical fiber and the host structure, respectively. This form of the coupling tensor has been independently verified[1,2] for surface-adhered sensors.

(2) The thermal mass of the fiber is negligible compared with that of the host.

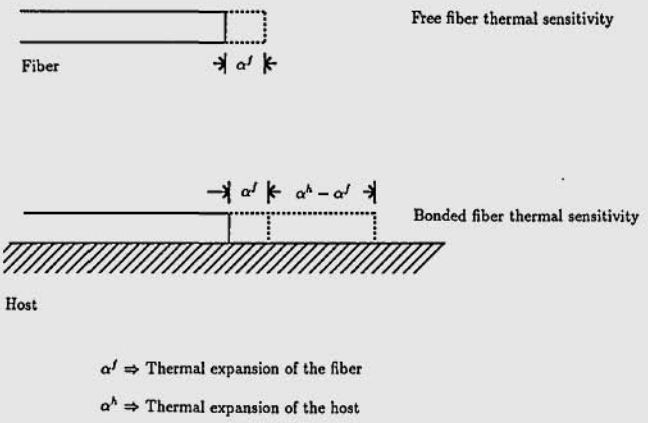

Fig. 1. Optical fiber bonded to a host material undergoing an unconstrained thermal expansion. The net phase is the sum of thermal strain and host-induced stress phase components.